Droplet Coalescence is Initiated by Thermal Motion (Supplemental Material)

Sreehari Perumanath,[1,*] Matthew K. Borg,[1] Mykyta V. Chubynsky,[2] James E. Sprittles,[2] and Jason M. Reese[1,†]

[1] *School of Engineering, University of Edinburgh, Edinburgh EH9 3FB, UK*
[2] *Mathematics Institute, University of Warwick, Coventry CV4 7AL, UK*

(Dated: November 29, 2018)

This Supplemental Material contains technical details that are complementary to the Letter. We discuss (i) the molecular dynamics simulation details and initial conditions, (ii) thermal fluctuations on liquid surfaces, (iii) the probable region of the onset of coalescence, (iv) bridge growth in the thermal regime, (v) calculations of thermal fluctuations on the surface of a thin cylinder, and (vi) the role of van der Waals interactions between the droplets.

SIMULATION DETAILS AND INITIAL CONDITIONS

Molecular dynamics (MD) simulations [1] of 3D and quasi 2D water droplets are performed in order to study the very early stages of droplet coalescence. MD is a particle based simulation tool in which the time evolution of a set of interacting particles is carried out by integrating their equations of motion: $\vec{F}_j = m_j \vec{a}_j$. Here $\vec{F}_j$ is the net force on an atom j whose mass is m_j and acceleration is $\vec{a}_j$. The force on any atom is the negative gradient of its potential energy function. In our systems, the effective potential between any two atoms, j and k is a combination of the shifted Lennard-Jones potential and electrostatic Coulombic interaction, given by

$$U_{jk} = 4\epsilon_{jk}\left[\left(\frac{\sigma_{jk}}{r_{jk}}\right)^{12} - \left(\frac{\sigma_{jk}}{r_{jk}}\right)^{6} - \left(\frac{\sigma_{jk}}{r_c}\right)^{12} + \left(\frac{\sigma_{jk}}{r_c}\right)^{6}\right] + \frac{1}{4\pi\epsilon_0}\frac{q_j q_k}{r_{jk}}, \tag{1}$$

where ϵ_{jk} is the van der Waals interaction energy between the atoms, σ_{jk} is the length parameter, r_{jk} is the distance between the atoms, q_j is the charge on atom j, ϵ_0 is the permittivity of the vacuum, and r_c=1.3 nm is the cut-off distance used. This value of r_c is typical in the literature for liquid-vapour systems [2]. Using a cut-off means that our description of interactions between the droplets is not fully correct at distances above r_c, as only Coulombic interactions are present. However, we argue in the final section of this Supplemental Material that this value is adequate for our purposes. Our studies are performed in a periodic box of size at least 4 times the diameter of the droplet in two directions. For quasi 2D droplets, the thickness of the box ($L = 4.3$ nm) is kept slightly larger than $3r_c$ so that a molecule will not interact with its own periodic image. Such a system essentially represents a particular section of a spherical droplet. Previous studies have shown that cylindrical droplets can qualitatively represent coalescence of spheres [3, 4]. The smallest diameter of the cylindrical droplets considered is 22.2 nm.

The TIP4P/2005 [5] model of the water with long-range Coulombic interactions (evaluated using the PPPM technique) is used in all our simulations. This is a rigid water model with 4 sites: one oxygen, two hydrogen and a massless site located below the oxygen along the HOH angular bisector. All simulations are performed in LAMMPS [6].

We begin the simulations by constructing a droplet; for the quasi 2D case a cylindrical water droplet of radius R is initialised with molecules that are randomly arranged, and an energy minimization is performed. Initial velocities corresponding to an absolute temperature of 300 K and zero net velocity of the entire droplet are assigned to every atom sampled from a Maxwell-Boltzmann distribution. The droplet is then equilibrated for ∼1000 ps, keeping the temperature constant using a Berendsen thermostat. The time step employed in our simulations is 0.002 ps. After equilibration, the thermostat is turned off, and the positions and velocities of all molecules are recorded at regular intervals of 4 ps for a further 2000 ps and the droplet radius is then determined (Fig. 1).

In order to generate the initial configuration of two droplets, to study their coalescence, two frames are taken from the above simulation, which are well separated in time (by at least 1000 ps) so that they can be considered as two independent droplets. Both droplets are then placed in a single simulation domain such that the minimum distance between the surfaces of the droplets is roughly the cut-off distance r_c. Again, we argue below that this initial distance is adequate, as only the later stages of approach are of importance. An initial droplet velocity of ±1 m/s towards each other is given to

both droplets. A similar methodology is also employed in studying the coalescence of 3D droplets. No thermostat is applied during the coalescence process.

During coalescence, all relevant physical data are stored every 0.04 ps. In order to identify the location of the bridge connecting the two droplets at any instant during coalescence, we divided the entire domain into square bins of length 0.25 nm and averaged the density in every bin for 0.8 ps. Then the bins whose density corresponds to the average of the combined liquid and vapor densities are identified as *equimolar points* and are used to identify the droplet interface and locate the position of the bridge between the droplets. By comparing Figs. 2(a) and 2(b), it can be seen that our code accurately resolves the free surface shape of the droplet.

THERMAL FLUCTUATIONS ON LIQUID SURFACES

The actual shape of a droplet is composed of a mean profile (circular in quasi 2D and spherical in 3D) and a fluctuating part caused by the thermal noise of the molecules at the interface. In Fig. 1, we show the equimolar points for the long-time averaged profile of a quasi 2D droplet of radius 11.1 nm, where the local density is the average of the liquid and vapor densities. The structure of the same droplet at a particular instant and the corresponding equimolar points are shown in Figs. 2(a) and 2(b), respectively. Due to the presence of the thermal capillary waves, at any given instant the interface deviates significantly from the mean profile. However, these fluctuations smooth out if the profile is averaged over a long period of time.

While thermal capillary waves increase the surface area of the droplet, the surface tension will act to reduce it. Capillary waves cause the interface to oscillate and can be represented by a sum of modes that are orthogonal to each other. For a large enough droplet, the fluctuations are small compared to the droplet size so the problem is linear; as a result, the oscillation of any interfacial point in the radial direction is distributed normally about its mean location. Figure 3 shows the probability distribution, $G(r)$, of the location of a particular interfacial point on a cylindrical droplet of radius R=11.1 nm and a fitted normal distribution.

For a planar interface, the capillary wave modes are plane waves characterized by a wave number q. From Fourier analysis [7, 8], the mean-square magnitude of the oscillation of the surface in the absence of an external field can be shown to be

$$\langle \zeta^2 \rangle_{pl} = \frac{k_B T}{2\pi\gamma} \ln\left(\frac{q_{\max}}{q_{\min}}\right), \qquad (2)$$

and the square-root of this equation is the standard deviation of the normally distributed oscillation of an in-

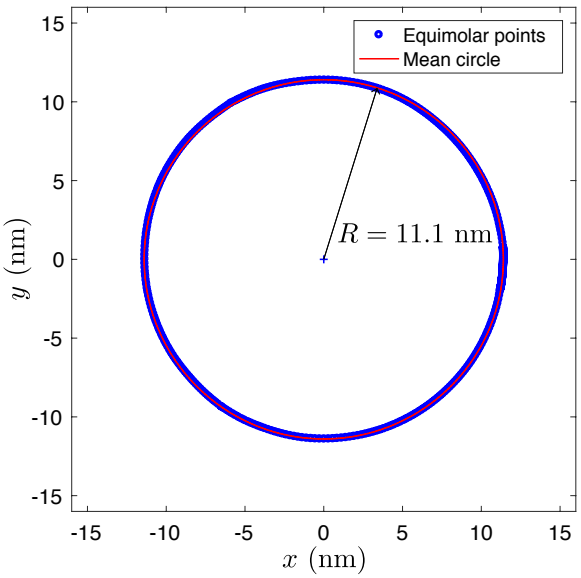

FIG. 1. Equimolar points and the mean surface for a long-time averaged droplet profile ($R = 11.1$ nm).

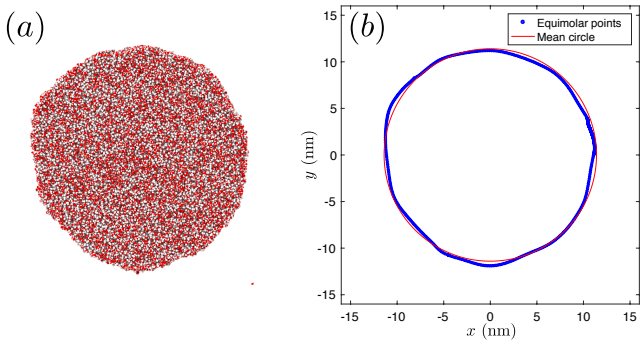

FIG. 2. (a) The structure of a quasi 2D droplet at an instant ($R = 11.1$ nm). Red spheres are oxygen and white ones are hydrogen atoms. (b) Equimolar points corresponding to (a) and the mean circle. At a particular instant, the profile is significantly different from the mean circular profile.

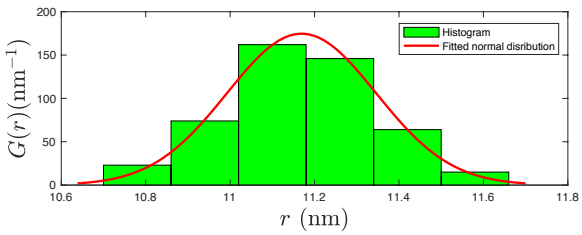

FIG. 3. The histogram of positions of a particular interfacial point on an R=11.1 nm cylindrical droplet and the fitted normal distribution.

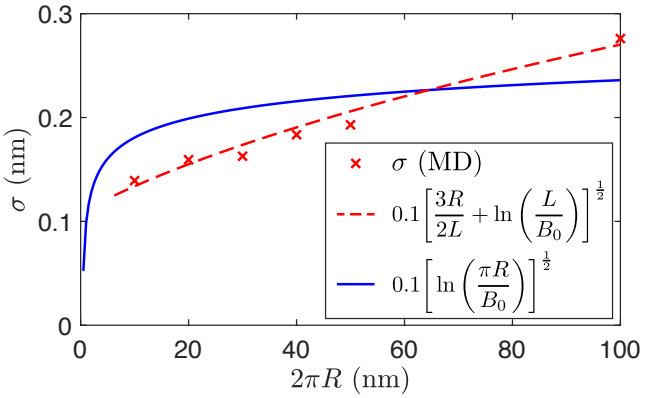

FIG. 4. Standard deviation σ of the local thermal fluctuations evaluated from MD simulations of cylindrical droplets varying with the circumference $2\pi R$. The broken red line is a fit to the red points in the form of Eq. (4) using only B_0 as a fitting parameter. Equation (4) is not applicable when $2\pi R < L$. The blue curve shows Eq. (3) with the same value of B_0 as used for the red line.

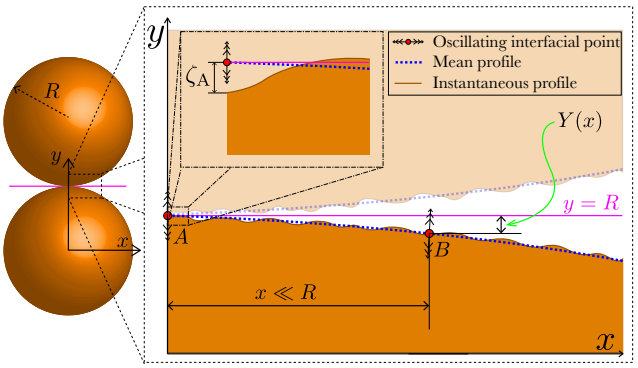

FIG. 5. Geometry of the coalescence onset problem for two 3D spherical droplets.

terfacial point about its mean position. In Eq. (2), k_B is the Boltzmann constant, T is the absolute temperature, γ is the liquid-vapour surface tension (65.4 mN/m for TIP4P/2005 water) and $q_{\max} = 2\pi/B_0$ signifies an upper cut-off for the wave number, beyond which it is meaningless to discuss fluctuations in terms of a set of continuous waves. A simple choice for B_0 is the size of a constituent molecule [7], radius of gyration or segment length in case of polymer chains [9]. On the other hand, in the absence of an external field, such as gravity, the lower cut-off for the wave number, $q_{\min}$, is characterized by the longest wave on the surface and depends on the system size, with an important assumption being that it is roughly the same in both dimensions.

For spherical surfaces of 3D droplets, we expect Eq. (2) to still apply, since for most modes (except those with the longest wavelengths) the surface is effectively flat on the scale of the wavelength, and the divergence for both $q_{\min} \to 0$ and $q_{\max} \to \infty$ indicates that both short- and long-wavelength modes are important. In this case, for the longest wave two wavelengths fit on the circumference of the sphere, and $q_{\min} \approx 2\pi/(\pi R)$. Therefore, the standard deviation of the thermal fluctuations is given by:

$$\sigma(R) = \sqrt{\langle \zeta^2 \rangle_{sph}} \approx \sqrt{\frac{k_B T}{2\pi\gamma}} \left[\ln\left(\frac{\pi R}{B_0}\right) \right]^{\frac{1}{2}}. \qquad (3)$$

It is assumed that $R \gg B_0$. Although $\sigma(R)$ is a diverging function of the radius, R, the divergence is very weak.

For quasi 2D droplets, the principal difference is that the surface characteristic dimension/length is very different in the axial and azimuthal directions. Assuming a thin disc geometry, i.e. $R \gg L$, the standard deviation of the oscillation of the surface is given by,

$$\sigma(R)_{cyl} = \sqrt{\langle \zeta^2 \rangle_{cyl}} = \sqrt{\frac{k_B T}{2\pi\gamma}} \left[\frac{3R}{2L} + \ln\left(\frac{L}{B_0}\right) \right]^{\frac{1}{2}}, \qquad (4)$$

(see final section for derivation). Unlike Eq. (3), Eq. (4) diverges quickly with increasing R while keeping L constant. For a water surface, we determined B_0 based on a fit to the dependence of the standard deviation of the surface fluctuations on the circumference, $2\pi R$, for quasi 2D systems, giving $B_0 \approx 1.2$ nm (see Fig. 4).

PROBABLE REGION OF THE ONSET OF COALESCENCE

Finding theoretically the distribution of locations at which coalescence initiates, taking surface fluctuations into account, is a complex problem deserving separate consideration. Only scaling estimates of the size of the coalescence onset region will be made here, by comparing the surface fluctuations in the region to the variation of the mean distance between the surfaces within that region due to their curvature.

Spherical droplets (3D)

Consider two spherical droplets of radius R approaching each other head-on (Fig. 5). The coalescence is most likely to be initiated on the line of approach. However, when surface fluctuations are accounted for, there is a possibility that a surface point B off the line of approach "overtakes" the point A on that line to initiate off-center coalescence. Suppose the distance between points A and B is $x \ll R$. Then the distance between the mean profiles at B is larger than that at A by

$$2Y(x) = 2(R - \sqrt{R^2 - x^2}) \approx x^2/R. \qquad (5)$$

Let the deviations of the profile of one of the droplets at a given instant of time at A and B be $\zeta_{\rm A}$ and $\zeta_{\rm B}$, respectively. It is reasonable to expect that the probability of coalescence at B is significant (comparable to that at A) if $\zeta_{\rm B}-\zeta_{\rm A}$ is likely to exceed $Y(x)$, or, in other words,

$$\left\langle(\zeta_{\rm B}-\zeta_{\rm A})^2\right\rangle \gtrsim Y^2(x) \approx \frac{x^4}{4R^2}. \tag{6}$$

The relative fluctuation $\zeta_{\rm B}-\zeta_{\rm A}$ is expected to be of the same order of magnitude as the typical fluctuations within a patch of size x, which, according to Eq. (2) and accompanying considerations, gives

$$\langle(\zeta_{\rm B}-\zeta_{\rm A})^2\rangle \approx \frac{k_BT}{2\pi\gamma}\ln\left(\frac{x}{B_0}\right). \tag{7}$$

The width of the distribution of coalescence onset locations, l_c, will be approximately equal to the value of x at which the left- and right-hand sides of Eq. (6) are equal, i.e.

$$\frac{k_BT}{2\pi\gamma}\ln\left(\frac{l_c}{B_0}\right) \approx \frac{l_c^4}{4R^2}, \tag{8}$$

so,

$$l_c \approx \left[\frac{2k_BT}{\pi\gamma}\ln\left(\frac{l_c}{B_0}\right)\right]^{1/4} R^{1/2}. \tag{9}$$

This is a transcendental equation that does not have a closed-form solution. However, in practice the logarithmic factor raised to a small power is of order unity, so for an order-of-magnitude estimate, it, along with the factor $(2/\pi)^{1/4}$, can be omitted, giving

$$l_c \approx \left(\frac{k_BT}{\gamma}\right)^{1/4} R^{1/2}. \tag{10}$$

Cylindrical droplets (quasi 2D)

For cylindrical droplets of axial length L, we use a similar approach. However, a complication is that instead of a single point A at which the mean profile of the droplet is closest to that of the other droplet, there is a line of such points. If point A is chosen arbitrarily on that line and point B on a line at distance x from the first line, the result for $\left\langle(\zeta_{\rm B}-\zeta_{\rm A})^2\right\rangle$ will depend on where exactly A and B are chosen with respect to each other: the closer the points, the smaller that expression is. It can then be argued that choosing A as close to B as possible (i.e., at distance x) is reasonable, since in order for coalescence to be initiated at B, the gap between the droplets at *all* possible A needs to be larger. The result will then depend on the relation between x and L. If $x<L$, then, similar to the spherical case, the relative displacement $\zeta_{\rm B}-\zeta_{\rm A}$ is of the same order of magnitude as typical displacements in a patch of size x in both dimensions. If, however, $x>L$, then the patch is still of size x in the azimuthal direction, but cannot exceed L in the axial direction. For such an asymmetric patch, we use our quasi 2D expression, Eq. (4), replacing R with $x/(2\pi)$. Then, arguing as before,

$$\frac{l_c^4}{4R^2} \approx \begin{cases} \frac{k_BT}{2\pi\gamma}\ln\left(\frac{l_c}{B_0}\right), & l_c<L, \\ \frac{k_BT}{2\pi\gamma}\left[\frac{3l_c}{4\pi L}+\ln\left(\frac{L}{B_0}\right)\right], & l_c>L. \end{cases} \tag{11}$$

Neglecting the logarithmic factor and term, and the numerical factors, gives

$$l_c \approx \begin{cases} \left(\frac{k_BT}{\gamma}\right)^{1/4} R^{1/2}, & l_c<L, \\ \left(\frac{k_BT}{\gamma L}\right)^{1/3} R^{2/3}, & l_c>L, \end{cases} \tag{12}$$

or

$$l_c \approx \begin{cases} \left(\frac{k_BT}{\gamma}\right)^{1/4} R^{1/2}, & R<L^2\left(\frac{\gamma}{k_BT}\right)^{1/2}, \\ \left(\frac{k_BT}{\gamma L}\right)^{1/3} R^{2/3}, & R>L^2\left(\frac{\gamma}{k_BT}\right)^{1/2}. \end{cases} \tag{13}$$

For the systems studied here, $L^2\left(\frac{\gamma}{k_BT}\right)^{1/2} \approx 73$ nm and they correspond to the top line of Eq. (13), which is the same expression as Eq. (10). For the three cylindrical droplets studied, $R=11.1$ nm, 20.1 nm and 58.5 nm, which correspond to $l_c=1.7$ nm, 2.2 nm and 3.8 nm, respectively.

Based on the above analysis, when two droplets of different radii coalesce, we expect no qualitative change in the results found in the current work. The effect of different radii may appear in two ways: 1) the droplets will now have different thermal fluctuation amplitudes, and 2) the gap thickness profile between the droplets will be modified, as this depends on the mean curvature between the droplets. For a realistic 3D system, the fluctuation amplitude depends only weakly on droplet sizes (Eq. (3)), so size will have a negligible effect on the overall process. As for the gap thickness, its effect is that the coalescence will correspond to that of two droplets of the same curvature, equal to the mean curvature of the actual droplets.

BRIDGE GROWTH IN THE THERMAL REGIME

As the total surface area decreases during droplet coalescence, the number of molecules at the interface will decrease as well. Figure 6(a) shows a snapshot of a typical coalescence between two R=11.1 nm cylindrical droplets when the bridge is still within l_T. The interface molecules at the same instant, identified by our interface tracking algorithm, are shown in Fig. 6(b). A criterion based on the total number of neighbors of a target molecule was used to identify the interface molecules. Typically, a bulk

water molecule will have roughly 310 neighbors within a sphere of radius r_c=1.3 nm, while an interface molecule will have fewer neighbors. Molecules with not more than 270 neighbors and not fewer than 5 gave the thickness of this layer of molecules close to the interfacial thickness of water (which is roughly 1 nm). The lower limit will disregard vapor molecules, if any, and a higher upper limit always identified a few molecules in the bulk.

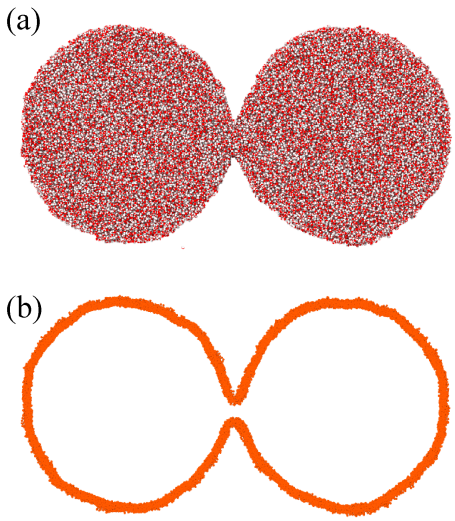

FIG. 6. (a) Snapshot of an instant of a typical coalescence process (quasi 2D; R = 11.1 nm) and (b) the corresponding interface molecules identified by our interface tracking algorithm.

Once the coalescence begins, the number of interface molecules starts to decrease, since many of these molecules will become bulk molecules during coalescence. For quasi 2D droplets, instead of the total number of interface molecules, we kept track of the variation of the number of interface molecules on either side of the contact point separately, as the bridges are often asymmetric. The variation of interface molecules on either side of the contact point is observed to be linear in time for cylindrical droplets. For spherical droplets, we studied the total number of interface molecules as a function of time since there is essentially a single bridge front, and the variation is non-linear (see Fig. 6 in the main paper).

We observe that during this early stage of coalescence, $r_b \leq l_T$, i.e. the system is in the thermal regime, during which time a relation between the bridge growth velocity v_b and the rate of change of the number of interface molecules near to that bridge front, $[dN/dt]$, can be obtained as follows. Let A denote the surface area of a single droplet and n_A denote the number of interface molecules per unit area. If the surface area of each droplet changes by ΔA, then the number of interface molecules changes by $2n_A\Delta A$. So,

$$dN/dt = 2n_A(dA/dt). \tag{14}$$

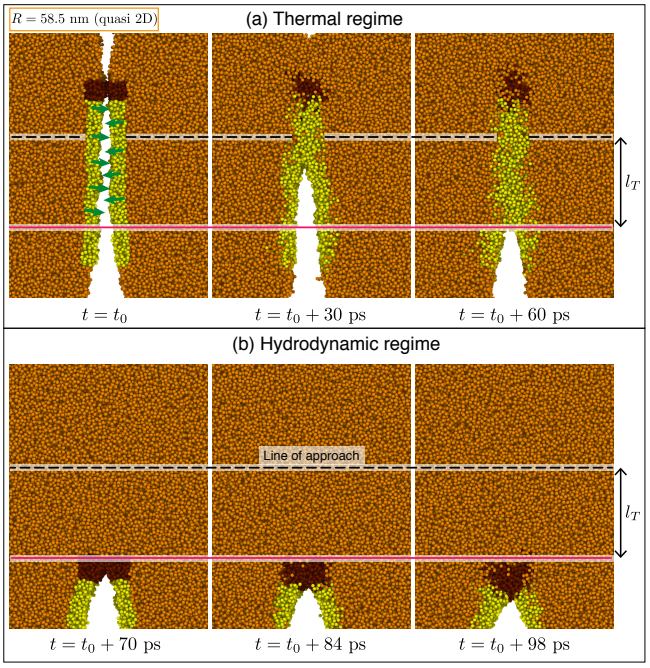

FIG. 7. Snapshots of the molecules in the thermal and hydrodynamic regimes during coalescence of two R=58.5 nm quasi 2D droplets.

On the other hand,

$$dA/dt = -(dr_b/dt)\Delta Z, \tag{15}$$

where ΔZ is the length of the bridge front over which molecular jumps occur. For the 3D spherical case, ΔZ is the circumference of the bridge. For quasi 2D systems with a single contact point between the droplets, we are able to track the variation of the number of interface molecules near a particular bridge front, i.e. on either side of the contact point separately, and consequently ΔZ is the length of a single front (i.e. L). Combining Eqs. (14) and (15), we get

$$v_b \equiv \frac{dr_b}{dt} \approx \frac{-dN/dt}{2n_A\Delta Z}. \tag{16}$$

From our MD results, we determine a length scale, l_T, up to which the bridge expands linearly through collective molecular jumps. The length scale l_T is identified as the point on the $r_b(t)$ plot above which the deviation from the initial linear behavior continually exceeds 0.5 nm. From our MD simulations we observe that l_T is seemingly captured by $2l_c$ for both 3D and cylindrical droplets, which is reasonable since both lengths are defined by thermal mechanisms.

Figure 7 shows the thermal and hydrodynamic regimes during the coalescence of two R = 58.5 nm cylindrical droplets. Only oxygen atoms are shown and some of them at the interface are colored differently for illustrative purposes. Oxygen atoms close to the bridge

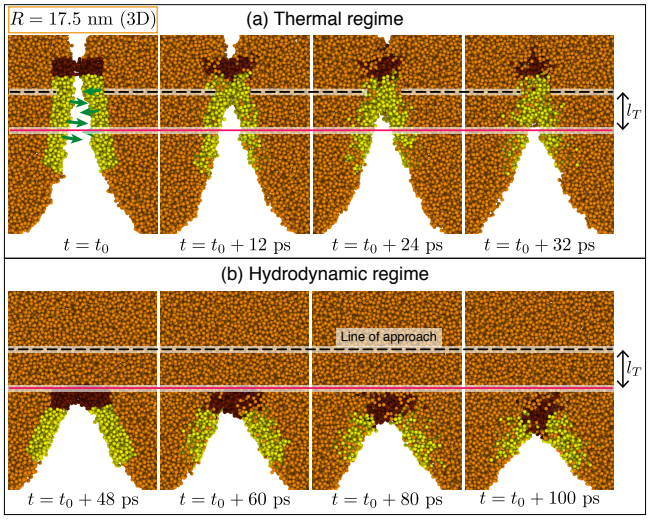

FIG. 8. Thermal and hydrodynamic regimes during coalescence of two R=17.5 nm spherical droplets.

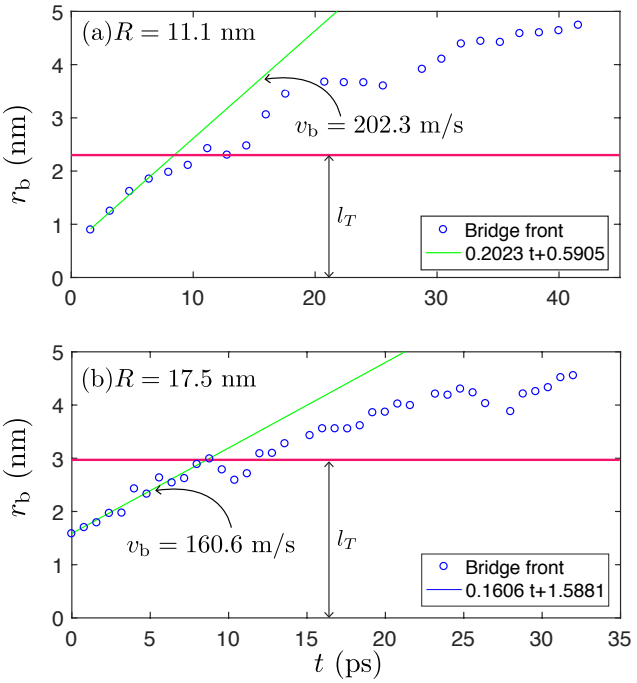

FIG. 9. Bridge growth during coalescence of (a) two R=11.1 and (b) two R=17.5 nm spherical droplets, evaluated from equimolar plots. The coalescence began close to the collision axis.

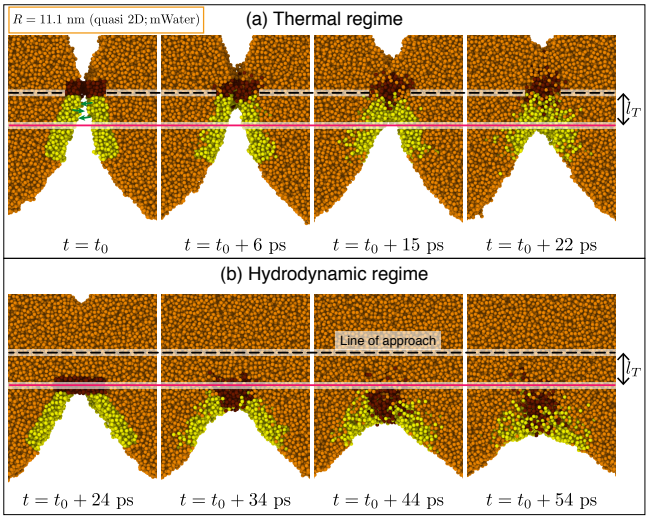

FIG. 10. Snapshots of the molecules in the thermal and hydrodynamic regimes during coalescence of two R=11.1 nm quasi 2D mW water droplets.

front are colored in maroon, and atoms near the confronting surfaces are colored in yellow. In the thermal regime, the bridge expands due to the confronting surfaces (yellow atoms) being drawn into each other. In the hydrodynamic regime, the bridge expands by the conventional bridging flow from under the bridge front (maroon atoms). In the snapshots for the 3D case (Fig. 8), some 'bulk colored' molecules are seen among the yellow and maroon molecules. These are molecules which entered the slice from outside because of self-diffusion.

Figure 9 shows the bridge growth as a function of time during the coalescence of two spherical droplets with (a) R=11.1 nm, and (b) R=17.5 nm. There is a characteristic change in the bridge expansion after the bridge passes the corresponding l_T, consistent with the change in mechanism of the bridge growth. Note that the reference time, t_0, shown in the snapshot figures is not the same as $t = 0$ in Fig. 9; t_0 is defined as the time at which the number of interface molecules at a particular bridge front starts to decrease and is determined by curve fitting (See Fig. 6 in the main paper). For a bridge to appear in the equimolar plots (which corresponds to $t = 0$ in Fig. 9), the bridge needs to have developed sufficiently so that there are enough molecules within it to evaluate a density profile.

In order to investigate the influence of inter-atomic potentials we use in MD simulations on the thermal regime, coalescence studies were carried out using a different model of water: the mW model [10], which in contrast to TIP4P/2005 uses a three-body potential among coarse-grained molecules and employs a shorter cut-off distance. Reassuringly, with the mW model, we still observe that the bridge initially grows as a result of collective molecular jumps, with little change in the thermal length scale (compare Figs. 10 & 11 here to Figs. 3 & 5(a) in the Letter). On the other hand, as expected, there are quantitative differences, in particular, in the bridge growth speed, which justifies using a more computationally expensive, but more accurate TIP4P/2005 model for our studies.

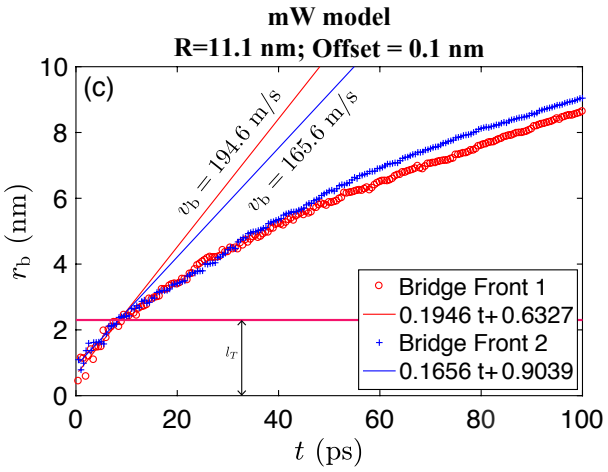

FIG. 11. Bridge growth during coalescence of two water droplets modelled using the mW model.

THERMAL FLUCTUATIONS ON THE SURFACE OF A LIQUID CYLINDER

In this section, we derive the mean-square displacement of the surface of a short cylinder due to thermal fluctuations (i.e. Eq. (4) above). This result is needed to obtain the value of the cutoff length B_0 from MD simulations, and is also used to derive the width of the distribution of coalescence onset locations.

Consider an incompressible liquid cylinder of radius R. Periodic boundary conditions with period L are assumed along the axis of the cylinder. Our consideration of thermal fluctuations of its surface uses an approach similar to that of Sides *et al.* [8] for a planar surface, where the fluctuations are expanded in eigenmodes and the equipartition theorem is utilized. However, there are two important differences. First, while in Ref. [8] the sum over the modes is replaced with an integral, which is valid for a surface with similar dimensions in the two directions, we retain the sum and analyze carefully under what conditions the replacement is possible. Second, in the case of a curved surface, special care needs to be taken to ensure that the eigenmodes preserve the volume.

In cylindrical coordinates, the shape of the surface of the cylinder is described by a function $r(z,\phi,t)$, where z is the coordinate along the axis ($0 \le z \le L$), ϕ is the azimuthal angle ($0 \le \phi \le 2\pi$), r is the radial distance of the surface from the axis, and t is the time. The surface area of the periodically repeated section of the cylinder is

$$A(t) = \int_0^L dz \int_0^{2\pi} d\phi \left(r^2 \left[1 + \left(\frac{\partial r}{\partial z} \right)^2 \right] + \left(\frac{\partial r}{\partial \phi} \right)^2 \right)^{1/2}, \tag{17}$$

and the volume is

$$V(t) = \frac{1}{2} \int_0^L dz \int_0^{2\pi} d\phi \; r^2. \tag{18}$$

We express the radial distance as

$$r(z,\phi,t) = R + \zeta(z,\phi,t), \tag{19}$$

and assume that the deviation ζ from the cylindrical shape is small ($\zeta \ll R$).

In the linear approximation free oscillations of the cylinder can be expanded into eigenmodes:

$$\zeta(z,\phi,t) \approx \sum_{n_z=1}^{\infty} \sum_{n_\phi=1}^{\infty} \zeta^{(1)}_{n_z n_\phi} + \sum_{n_z=1}^{\infty} \sum_{n_\phi=0}^{\infty} \zeta^{(2)}_{n_z n_\phi} + \sum_{n_z=0}^{\infty} \sum_{n_\phi=1}^{\infty} \zeta^{(3)}_{n_z n_\phi} + \sum_{n_z=0}^{\infty} \sum_{n_\phi=0}^{\infty}{}' \zeta^{(4)}_{n_z n_\phi}, \tag{20}$$

where

$$\zeta^{(1)}_{n_z n_\phi}(z,\phi,t) = a^{(1)}_{n_z n_\phi} \sin \frac{2\pi n_z z}{L} \sin n_\phi \phi, \tag{21}$$

$$\zeta^{(2)}_{n_z n_\phi}(z,\phi,t) = a^{(2)}_{n_z n_\phi} \sin \frac{2\pi n_z z}{L} \cos n_\phi \phi, \tag{22}$$

$$\zeta^{(3)}_{n_z n_\phi}(z,\phi,t) = a^{(3)}_{n_z n_\phi} \cos \frac{2\pi n_z z}{L} \sin n_\phi \phi, \tag{23}$$

$$\zeta^{(4)}_{n_z n_\phi}(z,\phi,t) = a^{(4)}_{n_z n_\phi} \cos \frac{2\pi n_z z}{L} \cos n_\phi \phi, \tag{24}$$

the coefficients $a^{(j)}_{n_z n_\phi}$ are time-dependent, and the prime in the last sum excludes the term with $n_z = n_\phi = 0$ as it corresponds to the uniform expansion or contraction of the cylinder and so does not preserve the volume.

When thermal fluctuations are considered, the coefficients a vary randomly in time and are uncorrelated, so

$$\langle a^{(i)}_{m_z m_\phi} a^{(j)}_{n_z n_\phi} \rangle \sim \delta_{m_z n_z} \delta_{m_\phi n_\phi} \delta_{ij}, \tag{25}$$

where $\langle \ldots \rangle$ denotes the time average and δ_{kl} is the Kronecker delta. However, it is important to note that perturbations of the form in Eqs. (21)–(24) do not preserve the volume exactly, with deviations quadratic in a. To ensure volume preservation, we replace Eq. (21) with

$$\zeta^{(1,2,3,4)}_{n_z n_\phi}(z,\phi,t) = a^{(1,2,3,4)}_{n_z n_\phi} \sin \frac{2\pi n_z z}{L} \sin n_\phi \phi - \Delta_{n_z n_\phi}(a^{(1,2,3,4)}_{n_z n_\phi}), \tag{26}$$

and similarly for Eqs. (22)–(24), where the Δ terms do not depend on z or ϕ and so correspond to uniform contraction (or expansion). By substituting these expressions into Eq. (19), expanding Eq. (18) to quadratic order in a and linear in Δ, and requiring that the volume remain equal to that of the unperturbed cylinder (i.e. $\pi R^2 L$), we obtain

$$\Delta_{n_z n_\phi}(a) = \begin{cases} \frac{a^2}{8R}, & n_z \neq 0 \text{ and } n_\phi \neq 0, \\ \frac{a^2}{4R}, & n_z = 0 \text{ or } n_\phi = 0. \end{cases} \tag{27}$$

While the Δ terms are quadratic in a and so at first sight seem negligible, this is not so, since the area change is quadratic in a, but linear in Δ.

Combining Eqs. (19), (20), (26) and (27), we can find the area change due to surface fluctuations using Eq. (17), expanding it to quadratic order in a and subtracting the area of the unperturbed cylinder (i.e. $2\pi RL$). We find that the contributions of different modes to the area change are additive, and are given by

$$\Delta A^{(j)}_{n_z n_\phi} = \begin{cases} \left(\frac{\pi^3 R n_z^2}{L} + \frac{\pi L (n_\phi^2-1)}{4R}\right)\left(a^{(j)}_{n_z n_\phi}\right)^2, & n_z \neq 0,\ n_\phi \neq 0, \\ \frac{\pi L (n_\phi^2-1)}{2R}\left(a^{(j)}_{n_z n_\phi}\right)^2, & n_z = 0, \\ \left(\frac{2\pi^3 R n_z^2}{L} - \frac{\pi L}{2R}\right)\left(a^{(j)}_{n_z n_\phi}\right)^2, & n_\phi = 0. \end{cases} \tag{28}$$

Equation (28) has two notable features. First, $\Delta A^{(j)}_{01} = 0$. This is expected, since the corresponding modes (there are two of them, $\zeta^{(3)}_{01}$ and $\zeta^{(4)}_{01}$) are pure translations in the directions transverse to the axis of the cylinder and so do not deform it. These modes need to be subtracted when calculating the displacement of the surface, so the corresponding terms should be deleted from Eq. (20). Second, $\Delta A^{(j)}_{10} < 0$ when $L > 2\pi R$, so the corresponding deformation decreases the surface energy. This is, of course, the well-known Plateau-Rayleigh instability [11]. When it is present, the deviation from the cylindrical shape can become arbitrarily large; we restrict ourselves to the case when the instability does not arise (as is indeed true for our quasi 2D MD systems). It is worth noting that neither of these important features is reproduced when the Δ term in Eq. (26) is not included.

Surface energy changes associated with the modes can be obtained by multiplying Eq. (28) by the surface tension γ. By equipartition, these energy changes are, on average, $k_BT/2$, which gives

$$\left\langle \left(a^{(j)}_{n_z n_\phi}\right)^2 \right\rangle = \begin{cases} \frac{2k_BT/(\pi\gamma)}{\frac{L}{R}(n_\phi^2-1)+\frac{4\pi^2 R}{L}n_z^2}, & n_z \neq 0,\ n_\phi \neq 0, \\ \frac{k_BT/(\pi\gamma)}{\frac{L}{R}(n_\phi^2-1)}, & n_z = 0, \\ \frac{k_BT/(\pi\gamma)}{\frac{4\pi^2 R}{L}n_z^2-\frac{L}{R}}, & n_\phi = 0. \end{cases} \tag{29}$$

Then, according to Eq. (20) with the $n_z = 0$, $n_\phi = 1$ terms removed, taking into account Eq. (25),

$$\langle \zeta^2 \rangle = \sum_{n_z=1}^{N_z}\sum_{n_\phi=1}^{N_\phi} \frac{2k_BT/(\pi\gamma)}{\frac{L}{R}(n_\phi^2-1)+\frac{4\pi^2 R}{L}n_z^2} + \sum_{n_z=1}^{N_z}\frac{k_BT/(\pi\gamma)}{\frac{4\pi^2 R}{L}n_z^2-\frac{L}{R}} + \sum_{n_\phi=2}^{N_\phi}\frac{k_BT/(\pi\gamma)}{\frac{L}{R}(n_\phi^2-1)}. \tag{30}$$

The result is independent of z and ϕ, which is expected, since all points on the surface are equivalent. Note that the upper summation limits have been made finite by introducing cutoffs N_z and N_ϕ. These cutoffs are important, because without at least one of them Eq. (30) would diverge. They are determined by the fact that below a certain length B_0 continuum fluid dynamics equations (on which the consideration here) is based cease to be valid. This length scale is typically comparable to the molecular size. The cutoffs then approximately correspond to the perturbations with wavelengths equal to this length scale, i.e.

$$N_z \approx \frac{L}{B_0}, \tag{31}$$

$$N_\phi \approx \frac{2\pi R}{B_0}. \tag{32}$$

Further progress can be made by assuming that the period in the axial direction L is much smaller than the radius R. We will also assume that B_0 is sufficiently small that $N_\phi \gg 1$. Then, since the last sum in Eq. (30) converges as $N_\phi \to \infty$, we can safely write

$$\sum_{n_\phi=2}^{N_\phi}\frac{k_BT/(\pi\gamma)}{\frac{L}{R}(n_\phi^2-1)} \approx \sum_{n_\phi=2}^{\infty}\frac{k_BT/(\pi\gamma)}{\frac{L}{R}(n_\phi^2-1)} = \frac{3k_BTR}{4\pi\gamma L}, \tag{33}$$

where the exact numerical value $\sum_{n=2}^{\infty} 1/(n^2-1) = 3/4$ has been used. The second sum

$$\sum_{n_z=1}^{N_z}\frac{k_BT/(\pi\gamma)}{\frac{4\pi^2 R}{L}n_z^2-\frac{L}{R}} \approx \frac{k_BTL}{4\pi^3\gamma R}\sum_{n_z=1}^{N_z}\frac{1}{n_z^2} < \frac{k_BTL}{4\pi^3\gamma R}\sum_{n_z=1}^{\infty}\frac{1}{n_z^2} = \frac{k_BTL}{24\pi\gamma R}, \tag{34}$$

which is much smaller than Eq. (33) and therefore negligible. Finally, considering the double sum, since changing n_ϕ by one makes a change in the expression under the sum that is small compared to the expression itself, the

sum over n_ϕ can be replaced by an integral:

$$\sum_{n_z=1}^{N_z}\sum_{n_\phi=1}^{N_\phi}\frac{2k_BT/(\pi\gamma)}{\frac{L}{R}(n_\phi^2-1)+\frac{4\pi^2R}{L}n_z^2} \approx \sum_{n_z=1}^{N_z}\int_{n_\phi=0}^{\infty}\frac{2k_BT/(\pi\gamma)}{\frac{L}{R}n_\phi^2+\frac{4\pi^2R}{L}n_z^2}dn_\phi = \frac{k_BT}{2\pi\gamma}\sum_{n_z=1}^{N_z}\frac{1}{n_z}. \quad (35)$$

Then

$$\langle\zeta^2\rangle \approx \frac{k_BT}{2\pi\gamma}\left[\frac{3R}{2L}+\sum_{n_z=1}^{N_z}\frac{1}{n_z}\right]. \quad (36)$$

The sum over n_z diverges in the limit $N_z\to\infty$, so N_z should be kept finite. If $N_z\gg 1$, then $\sum_{n_z=1}^{N_z}1/n_z\approx \ln N_z\approx\ln(L/B_0)$, and the final result is

$$\langle\zeta^2\rangle \approx \frac{k_BT}{2\pi\gamma}\left[\frac{3R}{2L}+\ln\frac{L}{B_0}\right], \quad (37)$$

which is our Eq. (4) above.

RELEVANCE OF VAN DER WAALS INTERACTIONS BETWEEN THE DROPLETS

In our theoretical consideration, we have assumed that the average shapes of the droplets remain spherical as they approach each other, and the fluctuations of the surfaces of the two droplets are independent of each other and of the distance between them. In reality, droplets in proximity to each other interact. First, they may interact hydrodynamically via the medium in which they move. In our simulation setup, however, the medium is the droplets' own vapor and has a very low density, so that interaction is clearly negligible. A more interesting effect is the van der Waals (vdW) interactions between the molecules belonging to different droplets. These interactions change the average shape of the droplets as they approach each other and also correlate the fluctuations of their surfaces and modify their spectrum. The most dramatic manifestation of the latter effect is an instability, in which fluctuations grow exponentially until the droplets touch.

Based on the fact that our simulation results generally agree with our theory and, in particular, there is no evidence of either a significant shape change or an instability, we have concluded that these effects probably do not play an important role under the conditions of our simulations. This is particularly interesting in view of the fact that it is the vdW-driven instability that is considered in many works (see, e.g., Ref. [12]) as giving rise to coalescence between the droplets. In fact, there is no contradiction, since our work differs from these previous ones in two respects: first, we simulate much smaller, nanoscale droplets, and second, as mentioned above, our simulations are carried out essentially in vacuum, which, by eliminating hydrodynamic interactions, affects the shape of the droplets and thus the effect of vdW interactions as well. The purpose of this section is to consider the role of these two factors. We take vdW interactions into account by introducing the disjoining pressure contribution to the normal stress at the boundary i.e

$$p_{\rm vdW}=-\frac{A_H}{48\pi H^3}, \quad (38)$$

where A_H is the material-dependent Hamaker constant, and H is one-half the separation between the surfaces.

We start by considering two very large volumes of liquid, separated by a vacuum gap between two planar parallel surfaces. Ignoring first the interactions between the surfaces, we assume that their thermal fluctuations are not large enough to bridge the gap (thus, strictly speaking, the surfaces cannot be infinitely large, since the fluctuations diverge as the size of the surface grows; however, this divergence is only logarithmic, so we will assume that the surfaces are infinite for all other intents and purposes). Nevertheless, when the interactions are "switched on", this system will still be unstable: the fluctuations with wavelengths above a critical one, λ_c, will grow exponentially. This critical wavelength corresponds to the surface perturbation mode for which the local changes in the disjoining pressure are exactly compensated by those in the Laplace pressure, which gives

$$k_c=2\pi/\lambda_c=\left(\frac{a_H}{\gamma}\right)^{1/2}, \quad (39)$$

where

$$a_H=\frac{A_H}{16\pi H^4} \quad (40)$$

For large H, the growth rates σ_k [defined so that the corresponding mode grows as $\exp(\sigma_k t)$] are so small that this growth may not matter for practical purposes. A general expression for the growth rate exists [13], but it is more convenient to use much simpler ones valid in the two limits, inertial and viscous, in both cases assuming $kH\ll 1$, and interpolate between them.

For small wavenumbers k, the growth rate is limited by the liquid inertia and is given by

$$\sigma_k=\left[\frac{(a_H-\gamma k^2)k}{\rho}\right]^{1/2}, \quad (41)$$

where ρ is the liquid density. For large k, it is limited by the viscosity μ and is

$$\sigma_k=\frac{a_H-\gamma k^2}{2\mu k}. \quad (42)$$

Both expressions vanish above k_c. Since σ_k grows as $k^{1/2}$ for small k and decreases to zero as $k \to k_c$, there is always a maximum, either at k at which Eq. (41) has a maximum ($k^i_{\max}$), or at the crossover k_x where Eqs. (41) and (42) are equal, whichever of the two values of k is smaller. The maximum of Eq. (41) is at

$$k^i_{\max} = \left(\frac{a_H}{3\gamma}\right)^{1/2}, \tag{43}$$

while the crossover is the solution of

$$\frac{4\mu^2}{\rho}k_x^3 + \gamma k_x^2 = a_H, \tag{44}$$

which is

$$k_x \approx \begin{cases} \left(\frac{\rho a_H}{4\mu^2}\right)^{1/3}, & a_H > \frac{\rho^2\gamma^3}{16\mu^4}, \\ \left(\frac{a_H}{\gamma}\right)^{1/2}, & a_H < \frac{\rho^2\gamma^3}{16\mu^4}. \end{cases} \tag{45}$$

The second line of this gives $k_x \approx k_c > k^i_{\max}$ and therefore is irrelevant. Then the value $k_{\max}$ at which the maximum rate is reached is either Eq. (43) or the top line of Eq. (45), i.e.

$$k_{\max} \approx \begin{cases} \left(\frac{\rho a_H}{4\mu^2}\right)^{1/3}, & a_H > \frac{27\rho^2\gamma^3}{16\mu^4}, \\ \left(\frac{a_H}{3\gamma}\right)^{1/2}, & a_H < \frac{27\rho^2\gamma^3}{16\mu^4}. \end{cases} \tag{46}$$

The corresponding maximum growth rate is

$$\sigma_{\max} \approx \begin{cases} \left(\frac{a_H^2}{2\mu\rho}\right)^{1/3}, & a_H > \frac{27\rho^2\gamma^3}{16\mu^4}, \\ \left(\frac{4a_H^3}{27\gamma\rho^2}\right)^{1/4}, & a_H < \frac{27\rho^2\gamma^3}{16\mu^4}. \end{cases} \tag{47}$$

There is a discontinuity, since an exact expression is used in the bottom line, but an approximate one in the top line, but it is relatively small and insignificant for our purposes. Note also that given Eq. (40), $\sigma_{\max}$ increases very rapidly when H decreases ($\propto H^{-8/3}$ in one regime and $\propto H^{-3}$ in the other). Individual modes grow quite rapidly, too: neglecting the γk^2 terms, the growth is $\propto H^{-2}$ in the inertial regime and $\propto H^{-4}$ in the viscous one.

Suppose now that the two liquid volumes approach each other with relative speed $2v$ so that H decreases linearly in time as $H_0 - vt$. Even with vdW interactions "switched off", the surfaces would touch before $H = 0$ due to fluctuations. Suppose this typically happens when $H = H_{\min}$. Then the question is whether the growth of the fluctuations due to the instability is significant before $H = H_{\min}$. We can still estimate the growth using Eqs. (41) and (42), keeping in mind that σ_k is now time-dependent. For the amplitude of a mode with wavenumber k we can write

$$a_k(t) \sim \exp\left(\int_0^t \sigma_k(t')dt'\right). \tag{48}$$

Because of the fast growth of σ_k with decreasing H, the value of σ_k at $H_{\min}$ dominates and the modes with the most growth are those with $k = k_{\max}(H_{\min})$. These modes grow by a factor

$$F_{\max} \simeq \exp[\sigma_{\max}(H_{\min})\Delta t], \tag{49}$$

where Δt is the effective time interval during which the growth rate is close to maximal and is

$$\Delta t = \alpha H_{\min}/v, \tag{50}$$

with α a numerical factor of order (but likely somewhat below) unity, e.g., $\alpha = 1/(\beta-1)$ for $\sigma_k(t) \propto (H_0/v-t)^{-\beta}$. Then, finally, the instability is not significant if

$$\sigma_{\max}(H_{\min})\Delta t < 1, \tag{51}$$

and significant otherwise.

The answer to the question above about significance of the instability depends on $H_{\min}$. For a rough estimate, we choose $H_{\min} = 1$ nm, which is the typical size of fluctuations of drop surfaces. Then for water ($\gamma = 65$ mN/m, $\mu = 10^{-3}$ Pa s, $\rho = 10^3$ kg/m^3, $A_H = 3.7 \times 10^{-20}$ J) we find that this corresponds to the top lines of Eqs. (46) and (47) (though close to the boundary between the regimes) and then $k_{\max} \approx 6\times10^7$ m^{-1}, $\sigma_{\max} \approx 6\times10^9$ s^{-1}. Then, according to Eq. (51) and assuming $\alpha = 1$, the instability is insignificant for $v > 6$ m/s, a moderate speed relevant experimentally, and the threshold may be even lower if $\alpha < 1$.

Are the above results relevant to spherical droplets of a finite size? The vacuum gap between the droplets is finite in extent and its width varies with the distance from the axis. This changes the surface modes and their spectrum. However, near the axis the gap width can be considered roughly constant. We define the "flat part" of the gap as that part of it where its width does not exceed $1 + s$ times the width on the axis, where $s \sim 1$. Then, assuming that H is much smaller than the radius of the droplet R, the radius of this "flat part" is

$$r_f \approx (2sRH)^{1/2}. \tag{52}$$

There will be modes oscillating many times within the "flat part"; these modes will have a well-defined wavenumber and for them the previous results obtained above for a flat infinite gap should remain valid. On the other hand, modes with wavelength above $\approx 4r_f$ (or $k < k_{\min} \approx \pi/(2r_f)$) do not exist. Then, if $k_{\min} < k_{\max}$ [Eq. (46)], the above results for the maximum growth rate (as well as those for significance of the instability) should remain valid; if, however, $k_{\min} > k_{\max}$, then the growth should be slower, being determined by the "flat-gap" rate for $k_{\min}$, rather than $k_{\max}$ (this rate may, in fact, be negative). The condition $k_{\min} < k_{\max}$ gives

$$\frac{\pi}{2r_f} < k_{\max}, \tag{53}$$

or

$$R > \frac{\pi^2}{8sHk_{\max}^2}. \tag{54}$$

For water and $H_{\min} = 1$ nm, we have obtained $k_{\max} \approx 6 \times 10^7$ m^{-1}, which, assuming $s = 1$, gives $R \gtrsim 300$ nm. Thus, our estimates should be roughly valid for macroscopic (e.g., mm-sized) droplets; however, for smaller droplets, like those used in our simulations, the rate should be slower and therefore even for slower approach speeds there should be no significant vdW effect, in agreement with our simulation results.

Another effect of vdW interactions that we have ignored so far is their influence on the average shape of the droplets. Since the disjoining pressure depends on the distance between the surfaces, its contribution is not constant on a spherical surface, which gives rise to pressure gradients. This creates flows that distort the surface. The process is similar to that giving rise to the instabilities that we have considered above, but with a specific length scale on the order of r_f (the size of the region on the surface where the interaction is the strongest). It is reasonable to assume then that the time scale of the process is similar to that for development of the instability with $k = k_{\min}$ (except perhaps with $\gamma \approx 0$, as the pressure gradient is created by vdW forces and is not initially counterbalanced by the Laplace pressure). This time scale is normally either comparable to or longer than the shortest time scale of the instability development and so this distortion process is never more important.

This explains how our results are different from what is commonly found in the literature where the effect of the vdW instability is dominant. In part, the difference does indeed arise from the fact that the growth rate is smaller for drops of nanometer size. However, a more important factor is that when drops collide in a medium, a thin film between them exists for a relatively long time (milliseconds for mm-sized drops), which is more than sufficient for the instability to develop, even if the growth rate is smaller than the value of $\sigma_{\max}$ quoted here due to the film being thicker than 1 nm.

The discussion above indicates that the biggest contribution of vdW interactions between the droplets arises within a short interval immediately preceding coalescence, of duration less than the time it takes the droplets to move a distance equal to the size of the fluctuations. Given that this size is somewhat below 1 nm for our droplets, the cut-off of 1.3 nm in our molecular dynamics simulations appears adequate.

* sreehari.dharmapalan@ed.ac.uk
† jason.reese@ed.ac.uk

[1] M. P. Allen and D. J. Tildesley, *Computer Simulation of Liquids*, 2nd ed. (Oxford University Press, Oxford, 2017).
[2] C. Vega and E. de Miguel, J. Chem. Phys. **126**, 154707 (2007).
[3] J. C. Pothier and L. J. Lewis, Phys. Rev. B **85**, 1 (2012).
[4] J. C. Burton and P. Taborek, Phys. Rev. Lett. **98**, 224502 (2007).
[5] J. L. Abascal and C. Vega, J. Chem. Phys. **123**, 234505 (2005).
[6] S. Plimpton, J. of Comput. Phys. **117**, 1 (1995).
[7] J. S. Rowlinson and B. Widom, *Molecular Theory of Capillarity* (Clarendon Press, Oxford, 1982).
[8] S. W. Sides, G. S. Grest, and M.-D. Lacasse, Phys. Rev. E **60**, 6708 (1999).
[9] A. Werner, F. Schmid, M. Müller, and K. Binder, Phys. Rev. E **59**, 728 (1999).
[10] V. Molinero and E. B. Moore, The Journal of Physical Chemistry B **113**, 4008 (2009).
[11] J. Eggers and E. Villermaux, Rep. Prog. Phys. **71**, 036601 (2008).
[12] A. K. Chesters, Trans. Inst. Chem. Eng. **69A**, 259 (1991).
[13] J. Lucassen, M. van den Tempel, A. Vrij, and F. T. Hesselink, Proceedings of the Koninklijke Nederlandse Akademie van Wetenschappen, Series B: Physical Sciences **73**, 109 (1970).